UC Irvine
UC Irvine Previously Published Works

Title
Propagation of neutralized plasma beams

Permalink
https://escholarship.org/uc/item/0vc6w13p

Journal
Physics of Fluids B: Plasma Physics, 2(6)

ISSN
08998221

Authors
Wessel, F. J
Rostoker, N.
Fisher, A.
et al.

Publication Date
1990

DOI
10.1063/1.859470

Peer reviewed

eScholarship.org Powered by the California Digital Library
University of California

P.M05

Propagation of Neutralized Plasma Beams

F. J. Wessel, J. J. Song, H. U. Rahman[a)],
G. Yur[a)], N. Rostoker, and R. S. White[a)]

Physics Department, University of California, Irvine, CA 92717

Abstract Beams of charge- and current-neutralized plasma will cross a transverse-magnetic field by a combination of collective-plasma processes. These processes were studied for a high -to-low beta ($\beta \equiv$ plasma energy density/magnetic field energy density) hydrogen-plasma beam injected into a vacuum transverse magnetic field with nominal parameters: $T_i \approx 1$ eV, $T_e \approx 5$ eV, $n \leq 10^{14}$ cm^{-3}, $v_i \leq 9 \times 10^6$ cm/s, $t_{pulse} < 70$ μs, $B_z \leq 300$ G. Plasma characteristics were measured for a wide beam, $a/\rho_i \leq 35$, and a downstream distance, $x \leq 300\ \rho_i$, where a is the beam radius, x is the downstream distance, and ρ_i is the ion gyroradius. A brief state of initial diamagnetic propagation is observed, followed by a rapid transition to $\underline{E}\times\underline{B}$ propagation. $\underline{E}\times\underline{B}$ propagation is accompanied by beam compression transverse to $\underline{B}$ with as much as a factor of four increase in density and a slight drift of the beam in the ion Lorentz force direction. As the magnetic field increases, the observed magnetization time decreases from that calculated using classical Spitzer conductivity, approaching an order of magnitude. This rapid magnetization can be accounted for using classical Hall conductivity, rather than invoking anomalous processes or instabilities to calculate the magnetization time.

a) Permanent address: IGPP, Univ. of CA, Riverside, CA 92521

1. INTRODUCTION

The magnetization time of a high-β plasma is a fundamental problem in plasma physics, yet is still poorly understood ($\beta \equiv$ plasma energy density/magnetic field energy density ≥ 1). Recent experiments, using intense ion beams and plasma gun beams demonstrate that fast magnetization can be accounted for by simply including classical-Hall effects.[1,2] Hall effects do not dissipate energy, yet can act as a vorticity-driven source of magnetic field that greatly increases the plasma-magnetization rate . Once a small component of magnetic field is present in a narrow high-beta beam the plasma quickly magnetizes and continues to propagate by the $\underline{E}\times\underline{B}$ drift. [3-5] Numerous experiments have revealed magnetization timescales which are orders of magnitude faster than classical and which are usually attributed to anomalous processes

or instabilities, especially for the case of collisionless plasmas. This understanding has application to the interpretation of high-β plasma experiments involving: active-space plasmas,[6-8] laser-produced,[9-12] gun-produced laboratory plasmas,[13-17] and high power opening switch plasmas,[18] as well as theoretical and computer simulation studies.[19-23]

This paper reports on the fast magnetization of a wide high beta plasma beam in the limit of long-range propagation, specifically in an attempt to clarify the importance of thermal and kinetic effects ($\beta_t \equiv 8\pi nkT/B^2$, $\beta_k \equiv 4\pi nMv^2/B^2$) and normalized beam width (a/ρ_i), relative to earlier experiments.[1,2,15] The next section details the experimental apparatus, Section 3 the experimental results, and Section 4 the results and conclusions. Cgs units are used throughout.

2. APPARATUS

Experiments were performed on the University of California, Riverside T-1 Space Simulation Facility (5.3-m long, 1.2-m ID fiberglass vacuum chamber, similar dimension stainless steel chamber, vacuum pressure $P \sim 3 \times 10^{-5}$ torr).[23] The experimental apparatus is illustrated in Fig.1. Magnetic-field coils are epoxied to the chamber exterior and produce a uniform transverse magnetic field in the range -300 to 300 G oriented along the z axis (driven by a 1200 μF, 3 kV capacitor bank, $t_{1/4} = 1$ ms). The plasma-beam is generated by a hydrogen-deflagration gun with coaxial-gun electrodes (ID of 7 cm, OD of 17 cm, and length of 100 cm) attached to a 450 μF, 7 kV capacitor bank (141 kA peak current, $t_{1/4} = 50$ μs risetime). Data was obtained by holding the magnetic field constant, firing the plasma gun several times for fixed

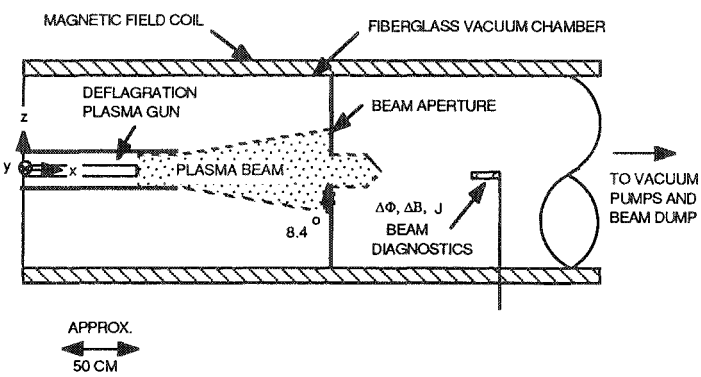

Figure 1. Schematic illustration of the experimental apparatus.

settings, and recording the response of various diagnostics. The plasma projects into the chamber along the x axis. Note that the Cartesian coordinate system is centered on the left-hand-side chamber flange.

Plasma-beam characteristics were sampled at three downstream locations: x = 206, 269, and 357 cm using probes inserted into the beam along the z axis: voltage-biased Faraday cups (- 78 V bias), magnetic probes (2-cm diameter, 25 turns of #9 gauge wire), floating-potential probes, and double-Langmuir probes (probe tips: two 0.5-mm diameter x 3-mm long platinum wires separated by 10 mm). Current probes monitor the gun-discharge current, field-coil current, and net-plasma current injected into the chamber.

The beam is injected through a collimating aperture (located at x = 170 cm and fabricated from plastic) prior to entering the drift space where the plasma parameters were measured. Use of a 7-cm diameter aperture resulted in a severe reduction in downstream beam energy, since the aperture was smaller than the ID of the gun. Therefore, all experiments where performed using either no aperture or with a 15-cm diameter aperture installed. The no-aperture plasma parameters at x = 269 cm and $B_z = 0$, are approximately: $T_i \approx 1$ eV (corresponding to a beam divergence, $\Delta\theta$ (FWHM)= 17°), $T_e \approx 5$ eV, $n_i = n_e \approx 10^{14}$ cm^{-3}, $v_i = v_e \approx 9 \times 10^6$ cm/s, $t_{pulse} <$ 70 μs.

3. RESULTS

Beam-current density was measured along the y and z axes at x = 357 cm in 5 cm increments to record the beam profile. Typical y-axis data for $B_z = 0$, 50 and 300 G, with the beam aperture installed, are shown in the dotted curves of Fig. 2. At $B_z = 0$ and 50 G the peak-current density is, J ~ 1.5 A/cm^2 and the FWHM beam width is Δy = 70 cm (~ $5.6\rho_i$). However, at $B_z = 300$ G the peak current density has shifted to the left of the y-axis origin and has increased to, J ~ 5.2 A/cm^2. The FWHM beam width was, Δy = 25 cm (~ $25\rho_i$), indicating that the beam was compressed from its zero-field profile. Measurements along the magnetic-field (z direction) revealed that the beam expanded freely, although the FWHM beam width decreased from Δz = 70 cm at 0, 50 G to Δz = 35 cm at 300 G. However, the apparent z-axis compression is only an artifact of the relative increase in current density resulting from y-axis compression. With no aperture installed the beam density was approximately three times greater than with the aperture, at all field strengths (c.f. dotted line in Fig 2 for zero-field data).

Deflection of the beam in the -y direction, y = 18 cm (~$15\rho_i$), is too small to be accounted for by the Lorentz force acting on a single ion, since the downstream location and deflection correspond to x = $250\rho_i$ (measured relative to the end of the gun electrodes). A slight deflection along the z axis was also observed of, z = 6 cm (< $5\rho_i$). Smaller deflections were observed closer to the gun, at x = 269 cm, albeit at higher current densities due to reduced beam expansion; at this location the non-apertured peak-current densities were, J = 4.3 and 11.7 A/cm^2 for B_z = 50 and 300 G, respectively.

Measurements of the time-of-flight (TOF) velocity as a function of magnetic field are displayed in Fig. 3 for the apertured beam (solid-line curves). The TOF velocity is obtained by noting the time delay between the leading-edge pulses of two Faraday cups located in sequential downstream ports and measures the average beam-front velocity between the two ports; it was not possible to measure the time-resolved bulk-velocity.

Generally as the magnetic field increases the TOF velocity decreases, indicating that the beam front decelerates. The largest deceleration is observed in the interval, x = 269-357 cm, as the field increases to 150 G. Above this value, as the field increases

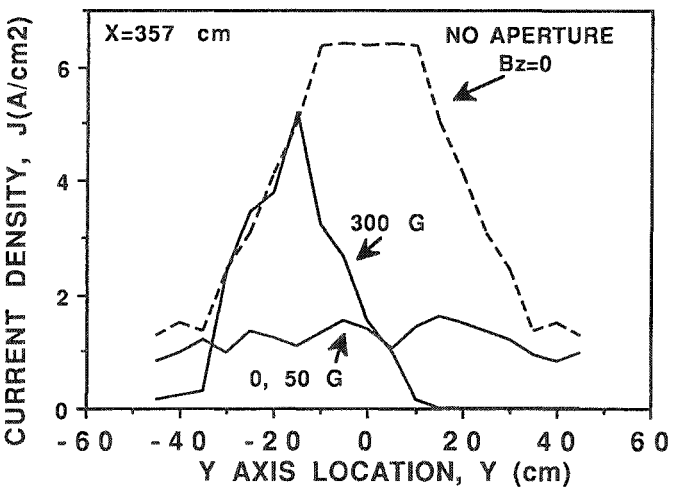

Figure 2. Y-axis current-density profiles at x = 357 cm for B_z = 0, 50 and 300 G; dotted lines are for the apertured beam and solid line with no aperture installed.

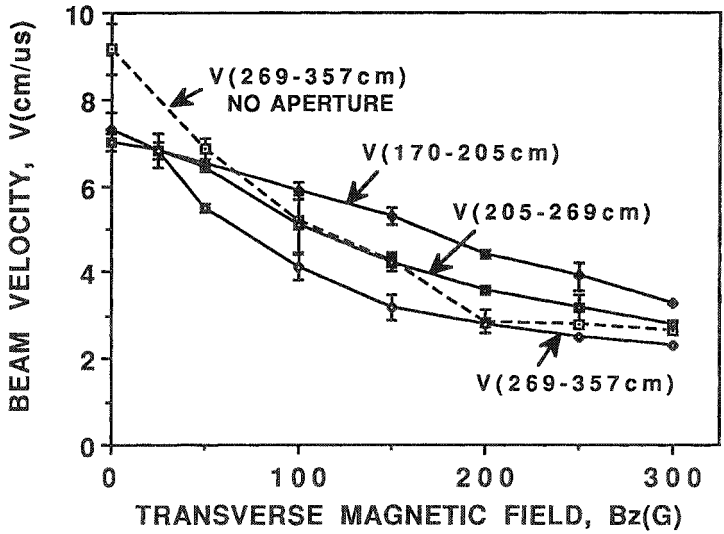

Figure 3. Time-of-flight ion velocity as a function of magnetic field; measured over the three intervals, x_1 = 170-205 cm, x_2 = 205-269 cm and x_3 = 269-357 cm. Solid curves - apertured beam, dotted curve - non apertured beam.

to 300 G, the TOF velocity approaches the asymptotic value, v_i = 2 cm/μs which is consistent with the magnetized ExB velocity estimated from floating-potential measurements. The non-apertured beam had a slightly higher initial velocity at lower fields, v_i = 9 cm/μs at B_z= 0 (c.f. dotted-line curve Fig. 3).

Prior to the arrival of the beam front, signals from diamagnetic probes inserted into the beam path displayed a transient increase above the ambient value, followed by a rapid decline to zero, and eventual return to the ambient value. The initial increase corresponds to compression of the ambient field ahead of the plasma beam while the decrease corresponds to the passage of the plasma-beam front over the magnetic probe. Diamagnetic currents which flow at the surface of the beam generate a magnetic field which adds vectorially to the vacuum field ahead of the beam and which cancels inside the beam.

Fast time resolution of the diamagnetic signal revealed that the initial increase in signal is accompanied by high-frequency noise and that the transition to diamagnetism occurred in approximately 0.5 μs at 50 G. From this the thickness of the beam-front diamagnetic-boundary layer is calculated to be of the order of $\lambda \approx 3.5$ cm. This value is an order of magnitude larger than the collisionless skin depth, c/ω_{pe}, and is more of the order of a hybrid skin depth, $c/\sqrt{\omega_{pe}\omega_{pi}}$. Higher field measurements revealed a thicker boundary layer, $\lambda \approx 30$ cm, and less diamagnetism.

Diamagnetic measurements for the apertured beam are displayed in Fig. 4 as a function of magnetic field for the three downstream locations. This Fig. shows that for $B_z < 150$ G, at x = 206, 269 cm, the beam remains largely unmagnetized, $B_{plasma}/B_z \leq 0.3$. Whereas for $B_z = 300$ G the levels of magnetization are, $B_{plasma}/B_z \sim 0.83$. Higher levels of magnetization are obtained further downstream, at x = 357 cm $B_{plasma}/B_z \sim 0.97$. Non-apertured data revealed even higher levels of diamagnetism; for $B_z = 300$ G, $B_{plasma}/B_z = 0.33, 0.57, 0.68$ for x = 206, 269, and 357, respectively.

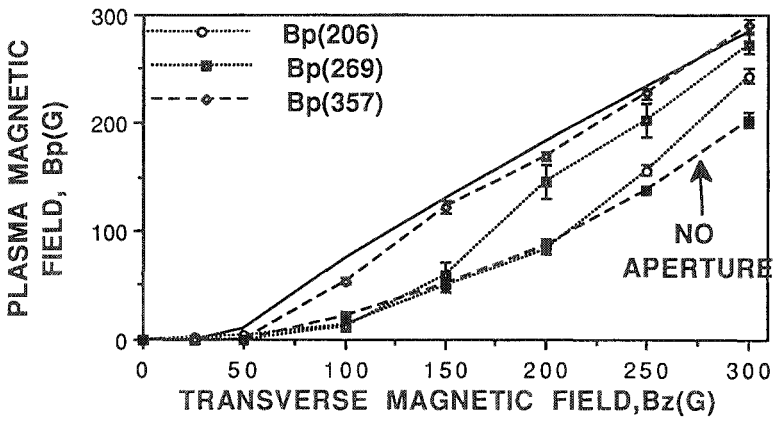

Figure 4. Magnetic field inside the plasma beam, B_{plasma}, as a function of applied magnetic field, B_z, at the three locations, x = 206, 269, 357 cm. The upper curve estimates the maximum plasma magnetic field from: $B_{plasma} = B_z\sqrt{1-\beta_t-\beta_k}$ (c.f. Section 4).

4. DISCUSSION

Qualitatively, beam propagation is dominated by diamagnetic effects at low magnetic fields and once the field penetrates, by the magnetized $\underline{E}x\underline{B}$ drift at high fields. As the plasma enters the field, shielding currents are induced at the beam surface that run the length of the beam and which produce an azimuthally periodic $\underline{J}x\underline{B}$ force in the y-z plane. This force is directed inward along the y axis and vanishes along the z axis. Beam compression observed at 300 G (c.f. Fig. 2) is a direct result of this pressure imbalance which persists until the magnetic field has penetrated. Similarly, deceleration in the -x direction results from the $\underline{J}x\underline{B}$ force at the beam front (Fig. 3). The net response of the plasma is to compress both radially and longitudinally, increasing the plasma temperature as the beam slows, and hence the ratio, β_t/β_k. Indeed, at 50 G the observed diamagnetic levels were too large to be accounted for by thermal effects alone, suggesting that a large amount of beam-kinetic energy was dissipated in excluding the magnetic field.

At the front of the high-beta beam energy density is conserved so that the following is satisfied,

$$B_{plasma} = B_z\sqrt{1-\beta_k-\beta_t}, \qquad (1)$$

valid for, $\beta_k, \beta_t \leq 1$. Values of B_p computed from this equation using experimental data for β_k and β_t, are plotted in Fig. 3 for x = 357 cm. Over the entire range of B_z there is good agreement with the measured value of B_{plasma}, confirming that the magnetic field penetrates an amount necessary to conserve energy density.

The magnetization time can be estimated from the 1-D linear diffusion equation,[24]

$$\frac{\delta B}{\delta t} = D\frac{\delta^2 B}{\delta y^2}, \qquad (2)$$

which has a solution,

$$B_{plasma}(y,t) = \frac{B_z}{2}\left[\mathrm{erfc}\,\frac{\frac{\Delta y}{2} - y}{2\sqrt{Dt}} + \mathrm{erfc}\,\frac{\frac{\Delta y}{2} + y}{2\sqrt{Dt}}\right]. \qquad (3)$$

In these equations erfc is the complementary error function, $D = c^2/4\pi\sigma$ is the magnetic-diffusion coefficient, $\sigma_c = (ne^2/m)\, t_{ei}$ is the classical Spitzer conductivity,[25] and $t_{ei} = 3.3\mathrm{x}10^4\ T^{3/2}/n$ is the electron-ion collision frequency. The magnetization time is $\tau = \Delta y^2/4D$.

Fig. 5 displays the magnetization time as a function of B_z , calculated using Spitzer conductivity, for the apertured-plasma parameters at x = 269 cm (upper curve).

Although the Spitzer magnetization time is independent of magnetic field and density, the slight decrease as a function of field displayed here reflects the decrease in (Δy) beam width noted experimentally.

It is difficult to obtain a precise experimental measure of the magnetization time due to a dynamic evolution in the plasma parameters, as the beam propagates. An approximate on-axis solution for B_p is obtained by keeping first-order terms in the series expansion for the error function,[26]

$$B_{plasma}(0,t) = B_z\{1 - \frac{4}{\pi} e^{-t/\tau}\} . \qquad (4)$$

Inverting this Eqn. for τ and using data from Figs. 3 and 4 for $B_{plasma}(t)$ we obtain the experimental magnetization times plotted in Fig. 6 as a function of B_z for the apertured beam (middle curve). Compared to the Spitzer-magnetization time we infer an order of magnitude faster magnetization for fields in the range, B_z = 150 -300 G. Furthermore, the experimentally-derived magnetization time appears to scale approximately as, $\tau \sim 1/B_z$.

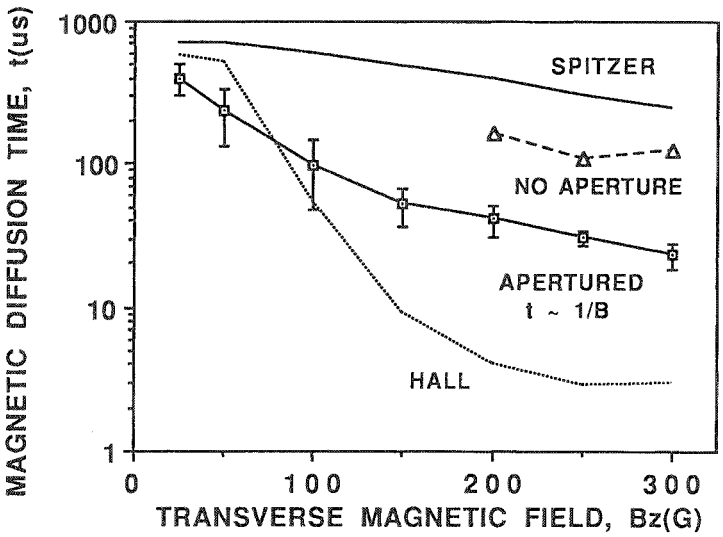

Figure 5. Magnetization times calculated using classical Spitzer conductivity (solid line) and using Hall conductivity (dotted line); apertured: solid line with data points, no aperture: dotted line with data points.

The magnetization time for the non-apertured beam is also displayed in Fig. 5 for the higher magnetic field values; at lower field the beam was essentially unmagneitzed and it was not possible to measure the magnetization time. Compared to the apertured-beam data the magnetization time is longer, reflecting the threefold increase in plasma density characterisitc of this configuration (c.f. Fig 2); differences in beam width were not a contributing factor.

Using Hall conductivity, $\sigma_H = \sigma_c\, \omega_{ce} t_{ei}/[1+(\omega_{ce} t_{ei})^2]$ instead of σ_c to estimate the magnetization time for the apertured beam, recovers the $1/B_z$ functional dependence. However, this results in another order of magnitude decrease in the magnetization time (dotted curve in Fig. 5) compared to the experimental value. Improved agreement may result by eliminating the (residual) thermal contribution to the diamagnetic signal. As well, an analytic solution to the nonlinear magnetic-diffusion equation would be beneficial.[20]

In conclusion this paper presents data on the long-range propagation of a plasma-beam in a transverse magnetic field for the specific case of a wide, low-to-high beta plasma. At high beta, $\beta \geq 1$, the observed magnetization time is nearly classical and the beam propagates by diamagnetic exclusion of the magnetic field, although the diamagnetic boundary-layer thickness is much smaller than classical. At low beta, $\beta \sim 0.1$, the beam propagates at nearly the <u>ExB</u> velocity and the magnetization time is as much as an order of magnitude faster than classical. A combination of these two magnetization states are observed at intermediate values of beta, $\beta = 0.1$ -1. Experimental results suggest that the magnetization time is dominated by classical Hall-conductivity effects and that anomalous diffusion processes and instabilities need not be invoked to describe the observed rapid magnetization rate. These results contrast with earlier results for a narrow beam, $a/\rho_i \leq 1$, where no propagation by diamagnetic exclusion of the magnetic field was observed for high β. The results for a narrow beam are qualitatively similar to the results for a low β beam involving very fast penetration of the magnetic field and <u>ExB</u> propagation.

The authors gratefully acknowledge stimulating and informative discussions with A. Fisher and W. Heidbrink (at UCI). Special thanks are due T. F. Chang (at UCI) for her assistance in measuring the beam-density profiles. This research was supported by the Air Force Office of Scientific Research (at UCI) and the National Aeronautics and Space Administration (at UCR).

5. REFERENCES

1. F.J. Wessel, N. Rostoker, A. Fisher, H. U. Rahman, and J. J. Song, Phys. Fluids **B2**, 1467(1990).
2. J. J Song, F. J. Wessel, G. Yur, H. U. Rahman, N. Rostoker, and R. S. White, Phys. of Fluids B, in press, June 1990.
3. G. Schmidt, Phys. Fluids **3**, 961(1960); Phys. Fluids **5**, 994(1962).
4. W. Peter and N.Rostoker, Phys. Fluids **25**, 730(1982).
5. F.J. Wessel and S. Robertson, Phys. Fluids **24**, 739(1981).
6. E. V. Mishin, V. Ya. Kapitanov, and R. A. Treumann, J.Geophys. Res. **91**, 10 183(1986).
7. G. Haerendel and R.Z. Sagdeev, Adv. Space Res. **1**, 29(1981).
8. See a series of articles in Nature **320**, 700(1986).
9. S. Okada, K. Sato, T. Sekiguchi, J. Phys. Soc. Japan **46**, 355(1970).
10. Y. P Zakharov, A. M. Orishich, A. G. Ponomarenko, V. G. Posukh, Sov. J. Plasma Phys. **12**, 674(1986).
11. B. H. Ripin, E. A. McLean, C. K. Manka, C. Pawley, J. A. Stamper, T. A. Peyser, A. N. Mostovych, J. Grun, A. B. Hassam, J. Huba, Phys. Rev. Lett. **59**, 2299(1987).
12. Yu. A. Bykovskii, V. P. Gusev, Yu. P. Kozyrev, I. V. Kolesov, V. B. Kutner, A. S. Pasyuk, and V. D. Peklenkov, Sov. Phys. JETP 69, 959(1989).
13. D.A. Baker and J. E. Hammel, Phys. Fluids **8**, 713(1965).
14. V. F. Demichev and V. M. Strunnikov, Sov. Phys. Doklady **8**, 484(1963) and V. G. Zykov, N. G. Smitsa, I. A. Stepanenko, V. T. Tolok, K. D. Sinelnikov, Sov. Phys. Tech. Phys **9**, 1094(1965).
15. F. J. Wessel, R. Hong, J. Song A. Fisher, N. Rostoker, A. Ron, R. Li, R. Y. Fan, Phys. Fluids **31**, 3778(1988) and R. Hong, F. J. Wessel, J. Song, A. Fisher, N. Rostoker, J. Appl. Phys. **64**, 73(1988).
16. M. P. Dejarlais, Phys. Rev. Lett. **59**, 2295(1987).
17. I. I. Demidenko, V. G. Padalka, B. G. Safronov, and K. D. Sinelnikov, Sov. Phys. Tech. Phys. **9**, 917(1965); **11**, 1354(1967); **16**, 1096(1972); N. A. Khizhnyak, I. I. Demidenko, N. S. Lomino, and V. G. Padalka, Sov. Phys. Tech. Phys. **13**, 1022(1969).
18. C. W. Mendel, Jr. and S. A. Goldstein, J. Appl. Phys. **48**, 1004(1977); B. V. Weber, R. J. Commiso, R. A. Meger, J. M. Neri;, W. F. Oliphant, and P. F. Ottinger, Appl. Phys. Lett. **45**, 1043(1984).
19. J. Koga, J. L. Geary, T. Fujinami, B. S. Newberger, T. Tajima, J. Plasma Phys. **42**, 91(1989).
20. . B. Newberger and N. Rostoker, J. Appl. Phys. **65**, 1874(1989).
21. M. Galvez and C. Barnes, Phys. Fluids 31, 863(1988).
22. J. Huba, J. G. Lyon, and A. B. Hassam, Phys. Rev. Lett. **59**, 2971(1987).
23. D.Winske, Phys. Fluids **B1**, 1900(1989).
24. P. J. Baum and A. Bratenahl, Geophys. Res. Lett. **9**, 435(1982).
25. H. S. Carslaw and J. C. Jaeger, Conduction of Heat in Solids, (Clarendon Press, Oxford, 1962) p. 54.
26. L. Spitzer, Physics of Fully Ionized Gases (Wiley, N. Y. 1962), p. 28.
27. H. Knoepfel, Pulsed High Magnetic Fields (North Holland Publishing Co., London, 1970) p. 60.

PN
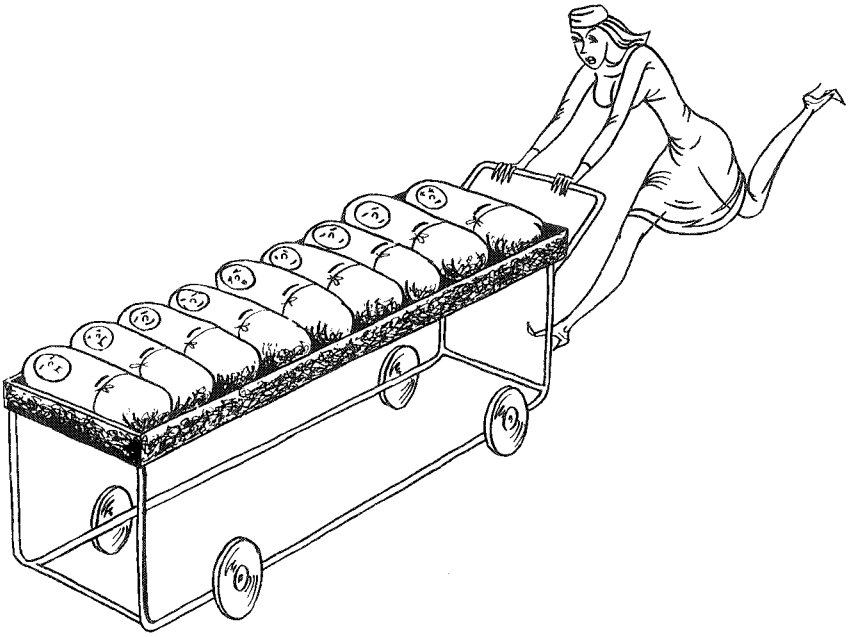
Electron beam generation and transport